Available online at www.sciencedirect.com

ScienceDirect

Procedia IUTAM 26 (2018) 184–193

Procedia IUTAM

www.elsevier.com/locate/procedia

IUTAM Symposium Wind Waves, 4–8 September 2017, London, UK

Generation method of wind waves under long-fetch conditions over a broad range of wind speeds

Naohisa Takagaki[a] *, Satoru Komori[b, c], Koji Iwano[d], Naoya Suzuki[e], Hiroshige Kumamaru[a]

[a]*Department of Mechanical Engineering, University of Hyogo, Himeji 671-2280, Japan*
[b]*Research Center for Highly-Functional Nanoparticles, Doshisha University, Kyotanabe 610-0394, Japan*
[c]*Center for Earth Information Science and Technology (CEIST), Japan Agency for Marine-Earth Science and Technology (JAMSTEC), Yokohama, 236-0001, Japan*
[d]*Department of Mechanical Systems Engineering, Nagoya University, Nagoya 464-8603, Japan*
[e]*Department of Mechanical Engineering, Faculty of Science and Engineering, Kindai University, Osaka 577-8502, Japan*

Abstract

It is important to develop a wave generation method for extending the fetch in laboratory experiments, because current laboratory studies are limited to fetch shorter than 100 m. Two wave generation methods are proposed for generating wind waves under long-fetch conditions in a wind-wave tank using a programmable irregular-wave generator. The first method is the spectral-model-based wave-generation method (SBWGM), which is appropriate at normal wind speeds for extending the fetch. The SBWGM also can be used at extremely high wind speeds if we know the spectral shape. In SBWGM, a conventional model of the wind-wave spectrum is used for the movement of the programmable irregular-wave generator. The second method is the loop-type wave-generation method (LTWGM), which can be used at wide range of wind speeds and is especially appropriate to be used at extremely high wind speeds, where the spectral shape is unknown. In LTWGM, the waves whose characteristics are most similar to the wind waves measured at the end of the tank are reproduced at the entrance of the tank by the programmable irregular-wave generator to extend the fetch. Water-level fluctuations are measured at both normal and extremely high wind speeds using resistance-type wave gauges. The results show that SBWGM can produces wind waves with a fetch over 500 m, but only at normal wind speeds. However, LTWGM can produce wind waves with long fetches exceeding the length of the wind-wave tank across a broad range of wind speeds, but considerable time is required to produce wind waves at long-fetch conditions, i.e. fetch over 500 m. It is observed that the wind-wave spectrum with a long fetch reproduced by SBWGM is consistent with that of the modelled wind-wave spectrum, although the generated wind waves are different from those in the open ocean because of the finite width of the tank. In addition, the fetch laws with significant wave height and period are confirmed for wind waves under long-fetch conditions. This implies that

* Corresponding author. Tel./fax: +81- 79-267-4834.
E-mail address: takagaki@eng.u-hyogo.ac.jp

Peer-review under responsibility of the scientific committee of the IUTAM Symposium Wind Waves.
10.1016/j.piutam.2018.03.018

the ideal wind waves under long-fetch conditions can be reproduced using SBWGM with the programmable irregular-wave generator.

Peer-review under responsibility of the scientific committee of the IUTAM Symposium Wind Waves.

Keywords: wave generation method; fetch

1. Introduction

It is very important to predict the momentum, heat, and mass transfers across the air-sea interface, because the transfer mechanism across this interface has a significant influence on the accuracies of future climate-change predictions, the intensity of the tropical cyclones, and other meteorological phenomena. The momentum, heat, and mass transfers across the wind waves have thus been the focus of many laboratory-experimental and numerical investigations [e.g. 1, 2, 3, 4, 5, 6, 7, 8, 9, 10, 11, 12].

Previous laboratory measurements have estimated this momentum transfer with a wind-wave tank [e.g. 1], and they have shown that the drag coefficient (C_D) increases monotonically with the 10-m wind speed (U_{10}) over a broad range of wind speeds. Here C_D represents the magnitude of the momentum transfer across the sea surface, which is given by:

$$\tau = \rho u^{*2} = \rho C_D U_{10}^2 , \tag{1}$$

where τ is the sea-surface wind shear stress, ρ is the air density and u^* is the air friction velocity. Conversely, recent laboratory results [6, 7] have shown approximately constant C_D values at extremely high wind speeds. Takagaki et al. [7, 13, 14] discovered that the breaking of wind waves occurs at extremely high wind speeds, causing C_D saturation. In fact, Uda [15] and Black et al. [16] reported that the sea surface appears to be flat above Douglas sea scale 9 and Beaufort scale 15, respectively.

It is important to examine the scalar transfer submodels used in the atmosphere-ocean general circulation model to predict future climate change and abnormal weather with high precision. The submodels have been proposed by many laboratory experiments using a wind-wave tank [e.g. 11, 17, 18, 19]. However, because these studies were carried out under short-fetch conditions (< 100 m), the momentum, heat, and mass transfers have not yet been observed under long-fetch conditions in laboratory experiments. Therefore, we must obtain the laboratory data at conditions of considerably longer fetch to discuss the similarity between the laboratory and field measurements; however, it is difficult to construct such a long wind-wave tank, especially for strong wind speeds.

Therefore, we propose an original technique for extending the fetch in a normal wind-wave tank to discuss the air-sea momentum and scalar transfer over a broad range of wind speeds, including extremely high wind speeds. These laboratory experiments at such long-fetch conditions will be useful in modelling small-scale air-sea coupling.

2. Experiment

2.1. Equipment and measurement methods

A large wind-wave tank (LWWT) [e.g. 20, 21] and a high-speed wind-wave tank (HSWWT) [e.g. 7, 11, 19] (Figure 1) were used in the experiments. The LWWT consisted of a glass test section that was 20.0 m long, 0.6 m wide, and 1.3 m high. The HSWWT consisted of a glass test section that was 15.0 m long, 0.8 m wide, and 1.6 m high. Wind waves were generated in the water tank, which was filled with filtered tap water, at U_{10} = 6.6, and 10.7 m/s with 2.5 % variation for the LWWT, and at U_{10} = 19.3, 32, and 42 m/s with 2.5 % variation for the HSWWT. Mechanical waves were generated using a programmable piston-type irregular-wave generator, consisting of a wave generating board, a servomotor (Mitsubishi Electric HC-SFS-152B for the LWWT and HC-SFS-352 for the HSWWT), a function generator (NF circuit WF1973), a wave gauge, a data recorder, and a computer. The wave- generating board was

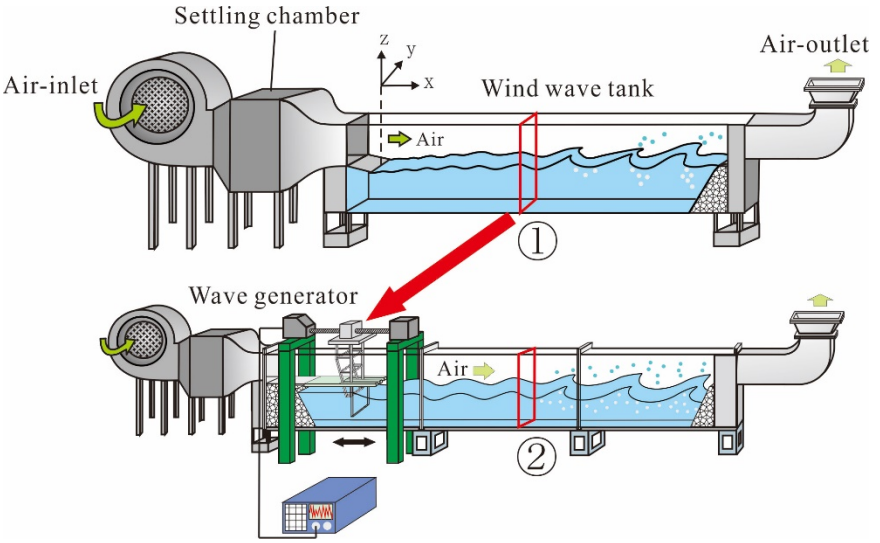

Fig. 1. Schematic diagram of high-speed wind-wave tank (HSWWT) and programmable irregular-wave generator for loop-type wave-generation method; (top) first wind waves generated by the fan; (bottom) second wind waves generated by the wave generator and fan along with first wind wave record.

an acrylic plate with a height, width, and thickness of 0.55 m, 0.598 m, and 0.015 m for the LWWT, and of 0.72 m, 0.78 m, and 0.02 m for the HSWWT, respectively. The center of the board stroke was set at x = -0.5 m under the entrance slope of both the LWWT and HSWWT. The maximum stroke was 0.2 m and 0.4 m for the LWWT and HSWWT, respectively.

A laser Doppler anemometer (Dantec Dynamics LDA) was used to measure the wind-velocity fluctuation. A high-power multi-line mode argon-ion (Ar^+) laser (Lexel model 95-7; λ = 488.0, 514.5 nm; 3 W power) was used. The Ar^+ laser beam was shot through the side glass-wall of the tank. Scattering particles of about 1 μm in diameter were generated by a fog generator (Dantec Dynamics F2010 Plus) and fed into airflow over the waves. The sampling frequency and sampling time were 500 – 5000 Hz and 240 s, respectively. The u^* in equation (1) was estimated using an eddy correlation method, such that $u^* = (-\langle u'v'\rangle)^{1/2}$ [e.g. 5, 22], where u' and v' are the streamwise and vertical air velocity fluctuations, respectively. Here, τ was estimated by extrapolating the measured values of the Reynolds stress $\langle u'v'\rangle$ to the mean surface at z = 0 m. Under neutral stratification, the wind-velocity profile over the rough boundary is expressed by the following logarithmic profile:

$$U(z)/u^* = \ln(z/z_0)/\kappa, \tag{2}$$

where $U(z)$ is the wind speed at elevation z, and κ (= 0.4) is the von Karman constant. From equations (1) and (2), C_D has a one-to-one correspondence with the roughness length (z_0) under neutral stratification:

$$\kappa C_D^{-1/2} = \ln(10/z_0), \tag{3}$$

Therefore, we evaluated z_0, C_D, and U_{10} using equations (1) – (3).

Water-level fluctuations were measured using resistance-type wave gauges (Kenek CHT4-HR60BNC). The resistance wire was placed in the water, and the electrical resistance at the instantaneous water level was recorded at 500 Hz for 600 s using a digital recorder (Sony EX-UT10). The energy of the wind waves (E) was estimated by integrating the spectrum of the water-level fluctuations over the frequency (f), where the peak frequency of the wind waves (f_m) was defined as the peak of the spectrum. To measure the wavelength (L_S) and the phase velocity (C_P) of the significant wind waves, another wave gauge was fixed downstream at Δx = 0.02 m (Runs 1-0, 2-0, and 3-0 to 3-

4), at Δx = 0.19 m (Runs 4-0 to 5-1), and at Δx = 0.2 m (Runs 1-M, 1-L, and 2-M), where Δx is the interval between the two wave gauges. The values of C_P were estimated using the cospectra method [e.g. 4].

The velocity and water level fluctuations measurements were conducted at a distance of x = 7.5 m from the edge (x = 0 m) of the entrance slope plate at the LWWT and at x = 5.5, 6.5, 8.5, or 11.5 m at the HSWWT (Figure 1). Wave absorbers were positioned at the inlet and outlet of the test section to prevent the reflection of surface waves.

2.2. Spectral-model-based wave-generation method (SBWGM)

Spectral models [e.g. 3, 23, 24, 25, 26] have been proposed for normal wind speeds. Therefore, a new method, referred to as the spectral-model-based wave-generation method (SBWGM), was employed to generate waves under long-fetch conditions in the LWWT by extending the actual fetch. First, the wind-wave spectrum at an arbitrary fetch was used as the input (Table 1) for the irregular-wave generator positioned at the inlet of the test section. Then, for a given initial fetch (500 m in this example), irregular wind waves were generated mechanically and forced with the fan, starting at an initial fetch $X_{initial}$ of 500 m and measured at fetch F = 507.5 m ($F = X_{initial} + X_{measure}$ = 500 + 7.5 = 507.5 m, where $X_{measure}$ is the measurement location of the waves for the wave analysis, see Table 1). In this study, the conditions with $F \leqslant$ 7.5 m and $F >$ 7.5 m are referred to as short- and long-fetch conditions, respectively, to distinguish pure wind-driven waves with a short fetch from the wind waves with a long fetch generated by SBWGM or loop-type wave-generation method (LTWGM).

Table 1. Measurement conditions. Wind waves at Runs 1-M, 1-L, and 2-M are generated by SBWGM. Wind waves at Runs 3-1 – 3-4, 4-1, 4-2, and 5-1 are generated by LTWGM. U_{10}: wind speed at a height of 10 m above the sea surface, N: number of loops in LTWGM, F: fetch (= $X_{initial}$ + $X_{measure}$), $X_{initial}$: extended length for spectrum method or LTWGM, $X_{measure}$: measurement location of waves for wave analysis this time, X_{loop}: measurement location of waves for LTWGM next time.

Run	U_{10}	N	F	$X_{initial}$	$X_{measure}$	X_{loop}
	[m/s]	[-]	[m]	[m]	[m]	[m]
1-0	6.6	-	7.5	-	7.5	-
1-M		-	507.5	500	7.5	-
1-L		-	2007.5	2000	7.5	-
2-0	10.7	-	7.5	-	7.5	-
2-M		-	507.5	500	7.5	-
3-0	19.3	0	6.5	-	6.5	11.5
3-1		1	17	11.5	5.5	8.5
3-2		2	25.5	11.5+8.5	5.5	8.5
3-3		3	34	11.5+8.5+8.5	5.5	8.5
3-4		4	42.5	11.5+8.5+8.5+8.5	5.5	-
4-0	32.0	0	6.5	-	6.5	411.5
4-1		1	17	11.5	5.5	8.5
4-2		2	25.5	11.5+8.5	5.5	-
5-0	42.0	0	6.5	-	6.5	11.5
5-1		1	17	11.5	5.5	-

2.3. Loop-type wave-generation method (LTWGM)

The above-mentioned spectral models proposed for normal wind speeds are not appropriate for the generation of wind waves at extremely high wind speeds, as the wind-wave properties are not well known. The LTWGM [27] is useful for generating waves under long-fetch conditions in the HSWWT. We only summarise the LTWGM manipulation here, since the manipulation is detailed in [27]. The LTWGM incrementally extends the actual fetch in a wind-wave tank. First, the wind waves are generated using a fan without the mechanical irregular-wave generator,

and the water-level fluctuation was measured at X_{loop} = 11.5 m (see upper image in Figure 1). The measured spectrum at $X_{initial}$ = 11.5 m is used as the input for the irregular-wave generator positioned at the inlet of the test section (lower image in Figure 1). Then, irregular wind waves were generated mechanically and forced with the fan, starting at $X_{initial}$ = 11.5 m and measured at F = 17 m ($F = X_{initial} + X_{measure}$ = 11.5 + 5.5 = 17 m, where $X_{measure}$ means the measurement location of waves for wave analysis, see Table 1). This iterative procedure is repeated to generate wind waves at different values of F. Wind waves were generated at F = 6.5, 17, 25.5, 34, and 42.5 m using LTWGM zero, one, two, three, and four times, respectively. However, wind waves at extremely high wind speeds were limited under F = 25.5 m because of the bottom-wall effects on wind waves. Note that the data from Runs 3-0 to 5-1 in Table 1 were reproduced using the measurements by [27].

2.4. Wave generation method

To generate wind waves using SBWGM, it is important that the power spectrum of the waves produced by the wave generator is the same as the input spectrum. The steps for employing SBWGM are similar to LTWGM [27], and are as follows.

The x-directional position, $P(t)$, of the wave-generating board is controlled using the servomotor and the function generator according to the following equation:

$$P(t) = \sum_i \frac{1}{2} L_i(f_i) \sin(2\pi f_i t + \theta_i), \tag{4}$$

where $L_i(f_i)$ is the stroke length at a neutral position (x = –0.5 m) and at an arbitrary frequency f_i, t is the elapsed time, and θ_i is the random phase. $L_i(f_i)$ is calculated using the single summation method [28]. Here, the energy of the waves $E_i(f_i)$, at an arbitrary frequency f_i is calculated by

$$E_i(f_i) = S_{\eta\eta}(f_i)\Delta f, \tag{5}$$

where $S_{\eta\eta}(f_i)$ is the power spectrum at an arbitrary frequency f_i and Δf is the frequency width for separating $S_{\eta\eta}(f_i)$ into frequency-direction bins, which is set at 0.001 Hz. Although f_i ideally ranges from zero to infinity, an actual wave generator has upper limits. Because the servomotor is not operational at frequencies above 3.2 Hz, the upper frequency limit of the wave generator is taken as 3.2 Hz. The relationship between the wave energy and the power spectrum is given by the following equations:

$$E_i(f_i) = S_{\eta\eta,model}(f_i)\Delta f \quad (0\ \text{Hz} < f_i < 3.2), \tag{6}$$

$$E_i(f_i) = 0 \quad (3.2\ \text{Hz} < f_i). \tag{7}$$

Here $S_{\eta\eta,model}$ is the power spectrum from the model proposed by [26]:

$$S_{\eta\eta,model}(f_i) = \alpha_D (2\pi)^{-4} g^2 f_m^{-1} f_i^{-4} \exp\left(-\left(\frac{f_i}{f_m}\right)^4\right) \gamma_D^{\Gamma}, \tag{8}$$

$$\Gamma = \exp\left(-\frac{(1-f_i/f_m)^2}{2\sigma_D}\right), \tag{9}$$

where α_D is the equilibrium range constant for the wind-wave spectrum, g is acceleration by gravity. Additionally, σ_D is the peak width parameter and γ_D is the peak enhancement factor. The relationship between the monochromatic wave energy $E_i(f_i)$, f_i, and $L_i(f_i)$ is calibrated through the preliminary experiment with monochromatic waves similar to that in [27], prior to generating the irregular waves. The position of the wave-generating board, $P(t)$, is calculated

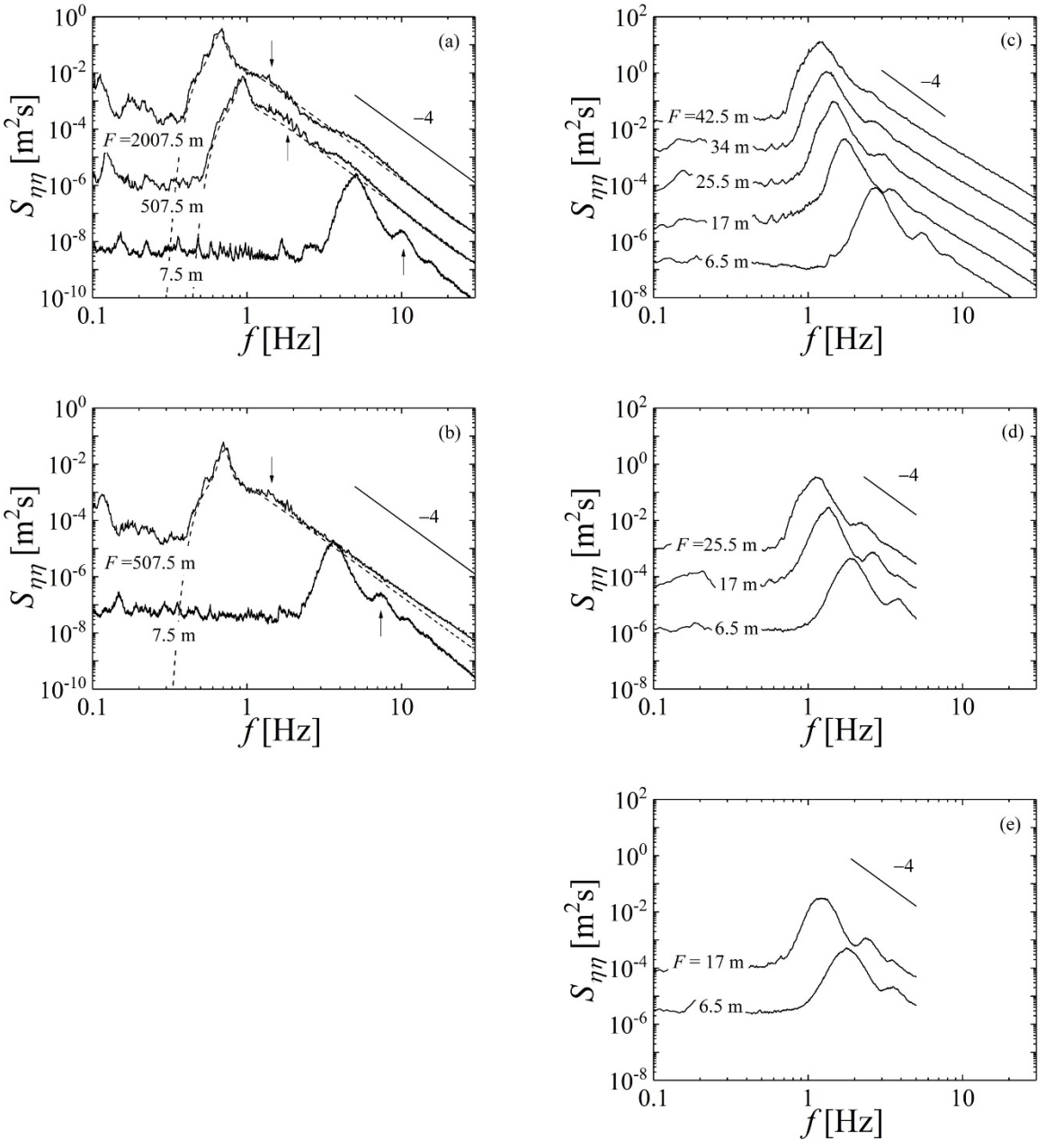

Fig. 2. Wind-wave Spectra $S_{\eta\eta}$ at (a – c) normal wind speeds (U_{10} = 6.6, 10.7, 19.3 m/s), and (d, e) extremely high wind speeds (U_{10} = 32.0, 42.0 m/s). Curves, from top to bottom, are for F = 2007.5, 507.5, and 7.5 m in Figure 2(a), F = 507.5, and 7.5 m in Figure 2(b), F = 42.5, 34, 25.5, 17, and 6.5 m in Figure 2(c), F = 25.5, 17, and 6.5 m in Figure 2(d), F = 17, and 6.5 m in Figure 2(e). Arrows in Figures 2(a, b) indicate secondary peaks. Spectra at high wind speeds (Figures 2d, 2e) are described for f = 5 Hz by removing impingement effects of droplets and bubbles on water-level measurements [e.g. 13]. Dashed curves represent a spectra calculated from a spectral model [26] in Figures 2(a – c). Spectra are offset for the clarity Figures 2(a – e). Solid lines represent a slope of –4 in Figures 2(a – e).

using the stroke length $L_i(f_i)$ at an arbitrary frequency from equation (4), and $L_i(f_i)$ is calculated from the wind-wave spectrum model. Therefore, by controlling $P(t)$, the wind waves at a fetch longer than the streamwise length of the LWWT can be generated by SBWGM.

3. Results and Discussion

To verify that the laboratory-generated wind waves using SBWGM are similar to those observed in the ocean, we have to investigate the wind-wave spectrum shape, fetch law, dispersion relation, and Toba's 3/2 power law [2], since these laws are observed for actual and pure wind-driven waves in both the ocean and the laboratory. Figure 2 shows the wind-wave spectra at U_{10} = 6.6, and 10.7 m/s for several fetch conditions. Note that the data in Figures 2(c – e) are reproduced using the measurements from [27]. It is observed that the wind-wave spectra (solid curves) generated by SBWGM correspond to those (dashed curves) proposed by [26]. This is attributed to the development of wind waves due to the increase in the fetch. While waves with frequencies higher than 3.5 Hz cannot be produced by the present wave generator, the slope at frequencies higher than f_m corresponds to a value of –4. Moreover, although the input spectral model [26] (see equations (8) and (9)) does not include a secondary peak at frequencies higher than f_m, the secondary peaks can be reproduced on the spectra by SBWGM. For example, the frequencies of the primary and secondary peaks are 1 and 2 Hz, respectively, at U_{10} = 6.6 m/s and F = 507.5 m. This implies that despite the generation of mechanical irregular waves by the wave generator, the wind shear itself produces a local equilibrium condition [3] between the wind shear and wind waves generated by SBWGM and the secondary peak.

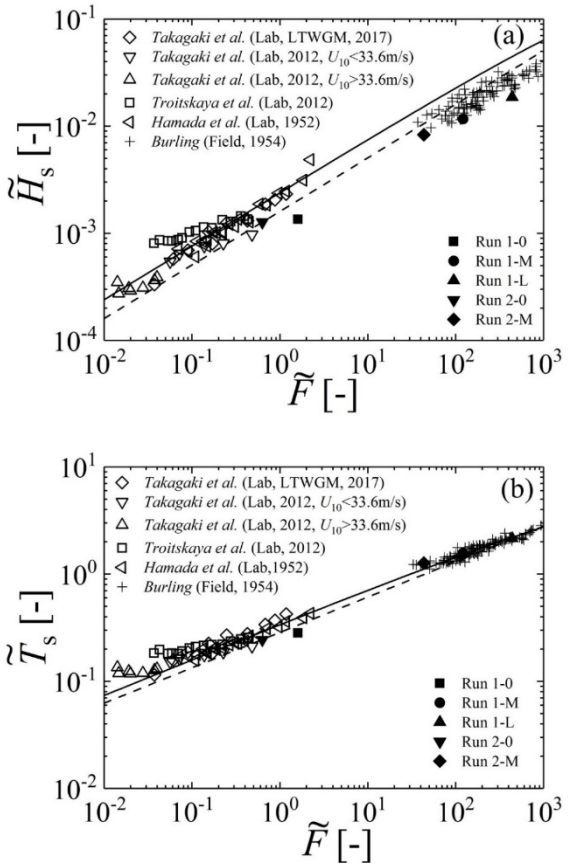

Fig. 3. Relationship between non-dimensional fetch $\widetilde{F}$ and (a) non-dimensional wave height $\widetilde{H_S}$, (b) non-dimensional wave period $\widetilde{T_S}$. Fetch, wave height, and wave period are normalized using wind speed U_{10} and gravity acceleration g. Solid curve: Wilson's formula IV [29]; Dashed curve: JONSWAP [25], both in (a, b). Laboratory values [10, 31] and field values [32] are added in the figure.

Therefore, it is concluded that SBWGM using the programmable irregular-wave generator can generate the ideal wind waves under long-fetch conditions. However, despite the fact that the input spectrum [26] decreases with a decrease in f for $f < f_m$, the SBWGM spectra level off due to the white noise. As mentioned in [27], the slope of LTWGM spectra at frequencies higher than f_m also correspond to a value of −4 (see Figures 2 (c – e)). Further details on the LTWGM spectra are in [27].

Figure 3 shows the relationships between the non-dimensional fetch $\widetilde{F}\ (= Fg/{U_{10}}^2)$ and both the non-dimensional wave height $\widetilde{H_S}(= H_S g/{U_{10}}^2)$ and non-dimensional wave period $\widetilde{T_S}(= T_S g/U_{10})$. Here the solid and dashed curves represent the fetch law from Wilson's formula IV [29] and JONSWAP [25], respectively. It is observed that the present plots, except Run 1-0, under both short- and long-fetch conditions, are concentrated around the previous plots and the solid and dashed curves, which implies that the SBWGM-generated wind waves follow the fetch law. Since the proposed fetch laws are proposed mainly based on field measurements, the plots at Run 1-0 (very short fetch) may scatter from the previous plots and empirical curves. The previous plots (Runs 3-0 to 3-4, symbol ∇) at $U_{10} < 33.6$ m/s are also concentrated around the solid and dashed curves, which implies that the LTWGM-generated wind waves also follow the fetch law, as mentioned in [27]. Figure 4 shows the dispersion relation and the relationship between the non-dimensional wave period T^* (= $T_S g/u^*$) and non-dimensional wave height H^* (= $H_S g/{u^*}^2$). Here, ω and k show the angular frequency and wavelength. In addition, the solid curves show the dispersion relation for a deep-sea wave [30] in Figure 4a and Toba's 3/2 power law [2] in Figure 4b, respectively. The figures show that the present plots under both short and long-fetch conditions (Runs 1-0 to 2-L) are concentrated around the solid curve, which

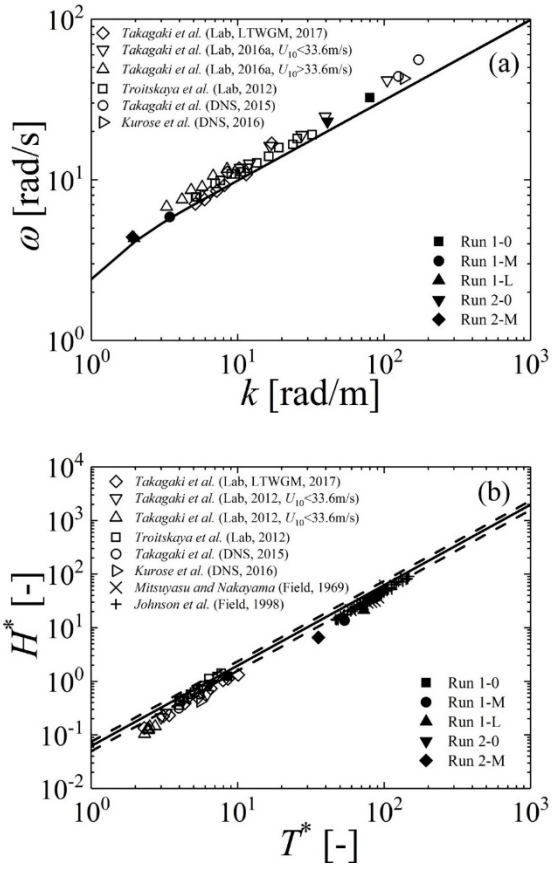

Fig. 4. (a) Dispersion relation, and (b) relationship between non-dimensional wave period T^* and non-dimensional wave height H^*. In (b), wave height and wave period are normalized using wind speed u^* and gravity acceleration g. Solid curve shows the dispersion relation and Toba's 3/2 power law [3] in (a, b), respectively. Dashed curves in (b) show the 20 % errors in Toba's 3/2 power law [3]. Laboratory values [10], predicted values [9, 12], and field values [33, 34] are added in the figure.

implies that the SBWGM-generated wind waves could be regarded as deep-sea waves following the Toba's 3/2 power law. The previous plots (Runs 3-0 to 3-4) are also concentrated around the solid curve, which implies that the LTWGM-generated wind waves follow the dispersion relation and Toba's 3/2 power law, as mentioned in [27].

Through the above verifications of the spectral shape, fetch law, dispersion relation, and Toba's 3/2 power law, it is confirmed that the ideal wind-driven waves under long-fetch conditions can be generated using SBWGM with the programmable irregular-wave generator. However, since SBWGM includes some of the same problems as LTWGM, and the wind waves generated by SBWGM do not correspond perfectly to those generated under the same field conditions. The differences between the present laboratory and field conditions are as follows: (1) The initial airflow entering the test section has a new turbulent boundary layer above the air-water interface under the present laboratory conditions; however, the boundary layer continues to develop under field conditions. (2) The present wave generator with SBWGM in the LWWT, with a width of 0.6 m, cannot produce the angular wave-wave spectrum, although the actual ocean waves spread to angular directions under field conditions. (3) Since there is the limitation due to the dispersion relation in the LWWT, with the depth of 0.7 m, we could not generate wind waves with the wavelengths longer than 1.4 m. These points should be improved before regarding the long-fetch laboratory conditions as true ocean conditions, but the present SBWGM is still helpful in laboratory experiments for modelling of small-scale air-sea coupling.

4. Conclusion

The abovementioned verifications of SBWGM in the LWWT, which is an original wind-wave generation technique, were demonstrated. Comparing SBWGM to LTWGM [27], the ideal wind waves at long-fetch conditions, such as 500 m or 2000 m, can be generated by SBWGM without the incremental steps required by LTWGM. Since SBWGM needs a conventional wind-wave spectrum, SBWGM cannot be applied to wind waves with an unknown wind-wave spectral shape at extremely high wind speeds. However, as incremental steps are required for LTWGM, it is difficult to generate the ideal wind waves at the long-fetch condition of 2000 m. If such wind waves are generated by LTWGM in a 10-m-long wind wave tank, ~ 200 incremental steps will be necessary. However, LTWGM does not need a conventional wind-wave spectrum, and can be applied to wind waves with an unknown wind-wave spectral shape and at extremely high wind speeds. In summary, SBWGM and LTWGM are suitable for wind-wave generation at normal and extremely-high wind speeds, respectively, although the generated wind waves are different from those in the open ocean because of the finite width of the tank. The present SBWGM, along with LTWGM, would be useful in laboratory experiments for modelling of small-scale air-sea coupling.

Acknowledgements

This work was supported by the Ministry of Education, Culture, Sports, Science and Technology (Grant-in-Aid Nos. 25249013 and 16K18015) and the Kawanishi Memorial ShinMaywa Education Foundation. We thank Prof. R. Kurose for useful discussions. We thank H. Muroya, M. Ishida, and S. Urakawa, for their assistance in conducting experiments at the LWWT, Kyoto University.

References

1. H. Kunishi, N. Imasato, On the growth of wind waves by high-speed wind flume (in Japanese), *Disaster Prevention Res. Inst. Annuals*, Kyoto Univ., Kyoto, 1966; **9**: pp. 667-676.
2. Y. Toba, Local balance in the air-sea boundary processes I. On the growth processes of wind waves, *J. Oceanogr. Soc. Japan*, 1972; **28**: 109–121.
3. Y. Toba, Local balance in the air-sea boundary processes III. On the spectrum of wind waves, *J. Oceanogr. Soc. Japan*, 1973; **29**: 209-220.
4. H. Mitsuyasu, Y. -Y. Kuo, A. Masuda, On the dispersion relation of random gravity waves. Part 2. An experiment, *J. Fluid Mech.*, 1979; **92**: 731-749, doi:10.1017/S0022112079000859
5. S. Komori, R. Nagaosa, Y. Murakami, Turbulence structure and mass transfer across a sheared air-water interface in wind-driven turbulence, *J. Fluid Mech.*, 1993; **249**: 161-183, doi:10.1017/S0022112093001120
6. M. A. Donelan, B. K. Haus, N. Reul, W. J. Plant, M. Stiassnie, H. C. Graber, O. B. Brown, E. S. Saltzman, On the limiting aerodynamic roughness of the ocean in very strong winds, *Geophys. Res. Lett.*, 2004; **31**: L18306, doi:10.1029/2004GL019460

7. N. Takagaki, S. Komori, N. Suzuki, K. Iwano, T. Kuramoto, S. Shimada, R. Kurose, K. Takahashi, Strong correlation between the drag coefficient and the shape of the wind sea spectrum over a broad range of wind speeds, *Geophys. Res. Lett.*, 2012; **39**: L23604, doi:10.1029/2012GL053988
8. N. Takagaki, R. Kurose, A. Kimura, S. Komori, Effect of Schmidt number on mass transfer across a sheared gas-liquid interface in a wind-driven turbulence, *Scientific Reports*, 2016; **6**: doi:10.1038/srep37059
9. N. Takagaki, R. Kurose, Y. Tsujimoto, S. Komori, K. Takahashi, Effects of turbulent eddies and Langmuir circulations on scalar transfer in a sheared wind-driven liquid flow, *Physics of Fluids*, 2015; **27**: 016603, doi:10.1063/1.4905845
10. Y. I. Troitskaya, D. A. Sergeev, A. A. Kandaurov, G. A. Baidakov, M. A. Vdovin, V. I. Kazakov, Laboratory and theoretical modeling of air-sea momentum transfer under severe wind conditions, *J. Geophys. Res.*, 2012; **117**: C00J21, doi:10.1029/2011JC007778
11. K. Iwano, N. Takagaki, R. Kurose, S. Komori, Mass transfer velocity across the breaking air-water interface at extremely high wind speeds, *Tellus B*, 2013; **65**: 21341, doi:10.3402/tellusb.v65i0.21341
12. R. Kurose, N. Takagaki, A. Kimura, S. Komori, Direct numerical simulation of turbulent heat transfer across a sheared wind-driven gas-liquid interface, *J. Fluid Mech.*, 2016; **804**: 646-687, doi:10.1017/jfm.2016.554
13. N. Takagaki, S. Komori, N. Suzuki, Estimation of friction velocity from the wind-wave spectrum at extremely high wind speeds, *IOP Conf. Series: Earth and Environmental Science*, 2016; **35**: 012009, doi:10.1088/1755-1315/35/1/012009
14. N. Takagaki, S. Komori, N. Suzuki, K. Iwano, R. Kurose, Mechanism of drag coefficient saturation at strong wind speeds, *Geophys. Res. Lett.*, 2016; **43**: 9829-9835, doi:10.1002/2016GL070666
15. M. Uda, *Marine Meteorology*, Tennensha, 1954; 297 page.
16. P. Black, R. W. Burpee, N. M. Dorst, W. L. Adams, Photo of the quarter – appearance of the sea surface in tropical cyclones, *Weather and Forecasting*, 1986; **1**: 102-107.
17. R. H. Wanninkhof, L. F. Bliven, Relationship between gas exchange, wind speed, and radar backscatter in a large wind-wave tank, *J. Geophys. Res.*, 1991; **96**: 2785-2796, doi:10.1029/90JC02368
18. S. Komori, R. Kurose, N. Takagaki, S. Ohtsubo, K. Iwano, K. Handa, S. Shimada, Sensible and latent heat transfer across the air-water interface in wind-driven turbulence, *GAS TRANSFER AT WATER SURFACES 2010* (Eds. S. Komori, W. McGillis, R. Kurose), Kyoto University Press, Kyoto, Japan, 2011; 78-89.
19. K. E. Krall, B. Jähne, First laboratory study of air–sea gas exchange at hurricane wind speeds, *Ocean Sci.*, 2014; **10**: 257-265, doi:10.5194/os-10-257-2014
20. K. Tanno, S. Ohtsubo, S. Komori, Effects of fetch on mass transfer across the air-water interface in wind-driven turbulence (in Japanese), *Transactions of the Japan Society of Mechanical Engineers, Series B*, 2007; **73**: 1510-1517, doi:10.1299/kikaib.73.1510
21. N. Takagaki, K. Iwano, E. Ilyasov, S. Komori, Y. Shirakawa, Development of an optical imaging technique for particle number density, *Journal of Fluid Science and Technology*, 2018; **13**: 17-00428, doi:10.1299/jfst.2018jfst0001
22. N. Takagaki, S. Komori, Effects of rainfall on mass transfer across the air-water interface, *J. Geophys. Res.*, 2007; **112**: C06006, doi:10.1029/2006JC003752
23. M. Phillips, The equilibrium range in the spectrum of wind-generated ocean waves, *J. Fluid Mech.*, 1958; **4**: 426-434, doi: 10.1017/S0022112058000550
24. W. J. Pierson, L. Moskowitz, A proposed spectral form for fully developed wind seas based on the similarity theory of S. A. Kitaigorodskii, *J. Geophys. Res.*, 1964; **69**: 5181-5190, doi:10.1029/JZ069i024p05181
25. K. Hasselmann, et al., Measurements of wind-wave growth and swell decay during the Joint North Sea Wave Project (JONSWAP), *Erganzugsh. Dtsch. Hydrogr. Z.*, 1973; **12**: 1-95.
26. M. A. Donelan, J. Hamilton, W. H. Hui, Directional spectra of wind generated waves, *Philos. Trans. R. Soc. London Ser. A*, 1985; **315**: 509–562, doi:10.1098/rsta.1985.0054
27. N. Takagaki, S. Komori, M. Ishida, K. Iwano, R. Kurose, N. Suzuki, Loop-type wave-generation method for generating wind waves under long-fetch conditions, *Journal of Atmospheric and Oceanic Technology*, 2017; **34**: 2129-2139, doi:10.1175/JTECH-D-17-0043.1
28. K. Hirayama, I. Miyazato, Generation method of directional random waves with arbitrary spectrum (in Japanese), *Report of the Port and Airport Researches*, 2009; **48**: 119-214.
29. B. W. Wilson, Numerical prediction of ocean waves in the north Atlantic for December, 1959, *Dt. Hydrogr. Z.*, 1965; **18**: 114-130.
30. H. Lamb, *Hydrodynamics*, 6th ed. Cambridge University Press, 1932.
31. T. Hamada, H. Mitsuyasu, N. Hase, An experimental study of wind effect upon water surface, *Rep. of Transportation Technical Research Institute*, 1953; **8**: 22 pp, doi:10.1049/cp.2014.1227
32. R. W. Burling, Surface waves on enclosed bodies of water, *Coastal Eng. Proc.*, 1954; **5**: 1-10, doi:10.9753/icce.v5.1.
33. H. Mitsuyasu, R. Nakayama, Measurements of waves and wind at Hakata Bay, *Rep. Res. Inst. Appl. Mech.*, 1969; **33**: 33-66.
34. H. K. Johnson, J. Hojstrup, H. J. Vested, S. E. Larsen, On the dependence of sea surface roughness on wind waves, *J. Phys. Oceanogr.*, 1998; **28**: 1702-1716, doi:10.1175/1520-0485(1998)028<1702:OTDOSS>2.0.CO;2